Electronic Supplementary Information

Mixed Ionic and Electronic Conducting Binder of PEDOT:PSS and Organic Ionic Plastic Crystals toward Carbon-Free Solid-State Battery Cathodes

Rafael del Olmo[1], Tiago C. Mendes[2], Maria Forsyth*[1,2,3] and Nerea Casado*[1]

[1]POLYMAT , University of the Basque Country UPV/EHU
Joxe Mari Korta Center, Tolosa 72, 200018 Donostia-San Sebastián, Spain

[2]Institute for Frontier Materials (IFM), Deakin University, Burwood, Victoria 3125, Australia

[3]Ikerbasque, Basque Foundation for Science, E-48011, Bilbao, Spain

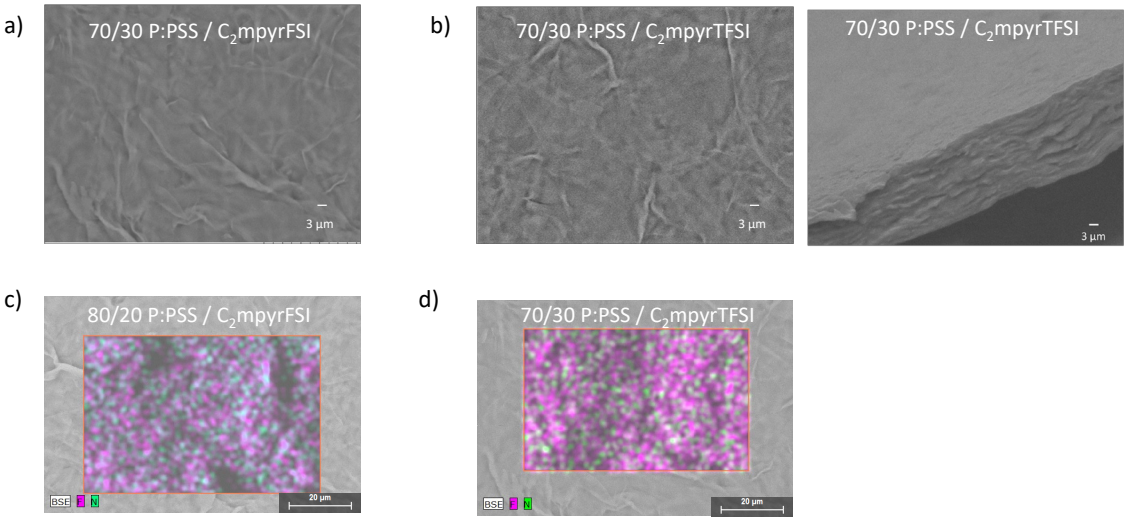

Figure S1. SEM images of a) 70/30 P:PSS / C_2mpyrFSI on the plane and b) 70/30 P:PSS / C_2mpyrTFSI on the plane and cross section. EDX images of the surface of the composites c) 80/20 P:PSS / C_2mpyrFSI and d) 70/30 P:PSS / C_2mpyrTFSI

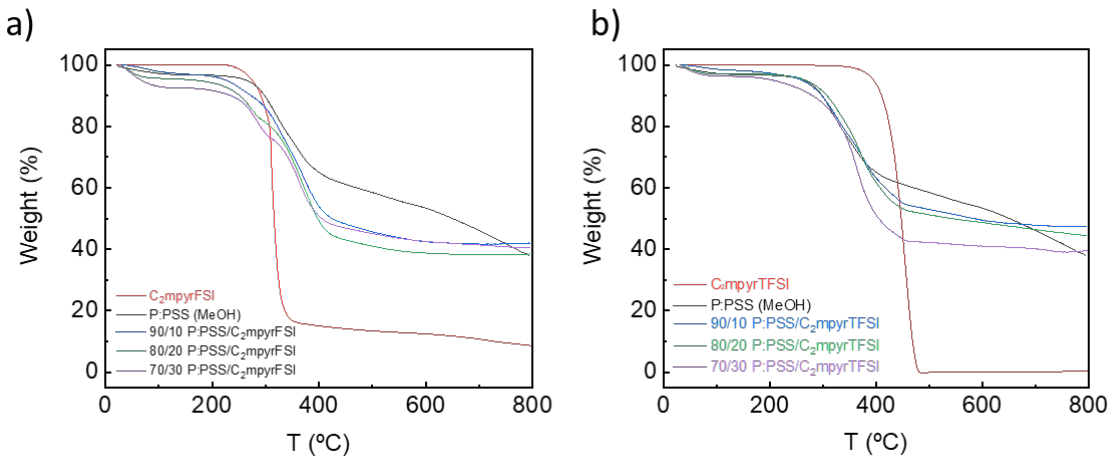

Figure S2. Thermogravimetric curves of neat P:PSS (MeOH) (black), OIPCs (red): a) C_2mpyrFSI, b) C_2mpyrTFSI, and their respective composites as follows the legends.

Ionic and electronic conductivity measurements:

On one hand, the influence of the electronic conductivity in the EIS measurements is negligible considering the low resistances generated by materials with conductivity values above 500 S/cm (considering also the dimensions of the sample). This assumption has been previously done in other works.[1] As an effect of the electronic conductivity, we can see closed semicircles in the Nyquist plots (Figure S3) since the interfacial capacitance is shunted by the electronic current.[2]

On the other hand, during 4-point-probe (4PP) measurements, the current is given purely through electronic conduction since the current delivered by the ions can be also neglected. DC polarization can be employed to determine both electronic and ionic conductivity by applying a constant current until stable current is reached. However, the most likely is that it will be limited by the ionic conductivity and high values of σ_{ionic} will be required to appreciate the difference.[3]

Therefore, similar values of electronic and ionic conductivities are needed to see a significant contribution of one over the other when using either 4PP or EIS.

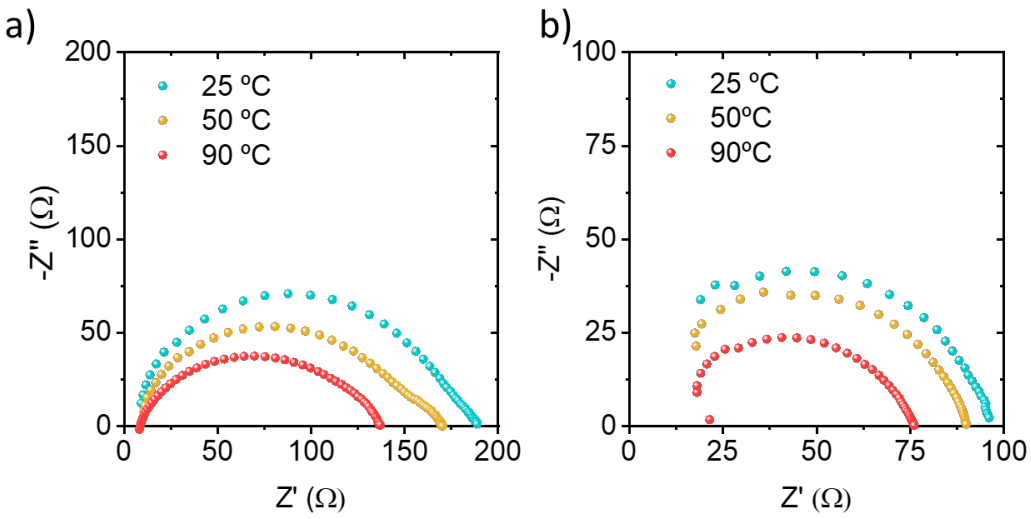

Figure S3. Nyquist plot of a) 80/20 P:PSS/C_2mpyrFSI and b)70/30 P:PSS/C_2mpyrTFSI at different temperatures

The activation energies (Ea) were calculated by using the Arrhenius equation:

$$\sigma = \sigma_0 \exp(\frac{-E_a}{k_B T})$$

where σ_0 is the dc conductivity of pre-exponential factor, T the absolute temperature, E_a the activation energy and k_B the Boltzmann constant.

Table S1. Activation energy of the ionic conductivity of PEDOT:PSS, C_2mpyrFSI, C_2mpyrTFSI and their composites.

	Activation Energy [KJ mol^{-1}]
PEDOT:PSS	4.9 ± 0.4
C_2mpyrFSI	12.9 ± 0.1
90/10	3.6 ± 0.2
80/20	1.9 ± 0.1
70/30	1.6 ± 0.3
C_2mpyrTFSI	11.4 ± 0.3
90/10	4.2 ± 0.2
80/20	5.2 ± 0.3
70/30	4.6 ± 0.4

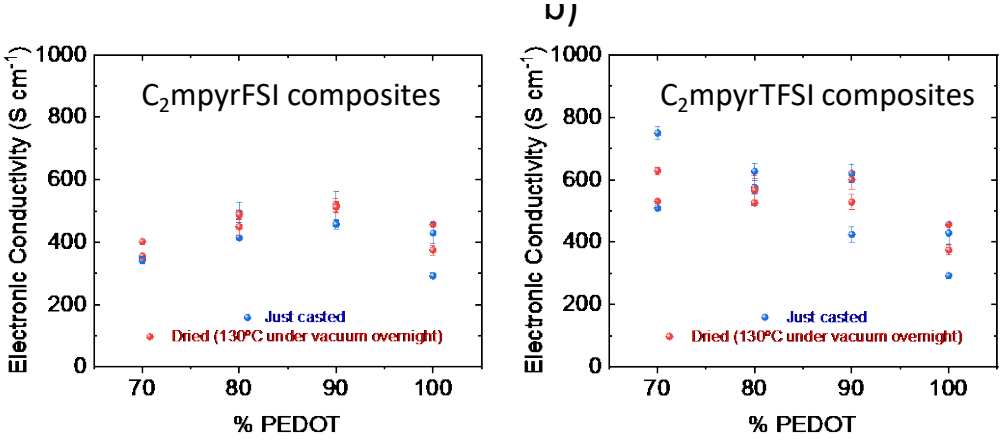

Figure S4. Electronic conductivity of P:PSS (MeOH), a) FSI and b) TFSI based composites dried at room temperature and after drying at 130ºC under vacuum overnight.

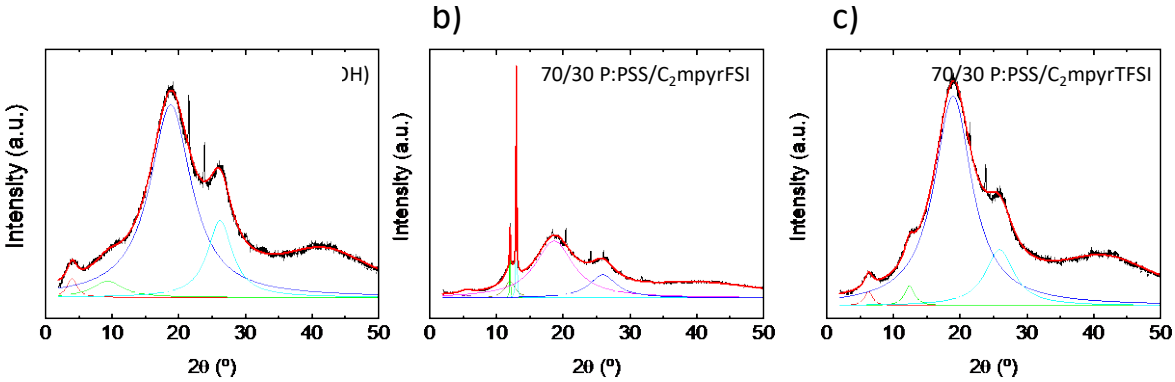

Figure S5. Deconvolution of the XRD patterns of a) P:PSS (MeOH), b) 70/30 P:PSS/C_2mpyrFSI and c) 70/30 P:PSS/C_2mpyrTFSI composites.

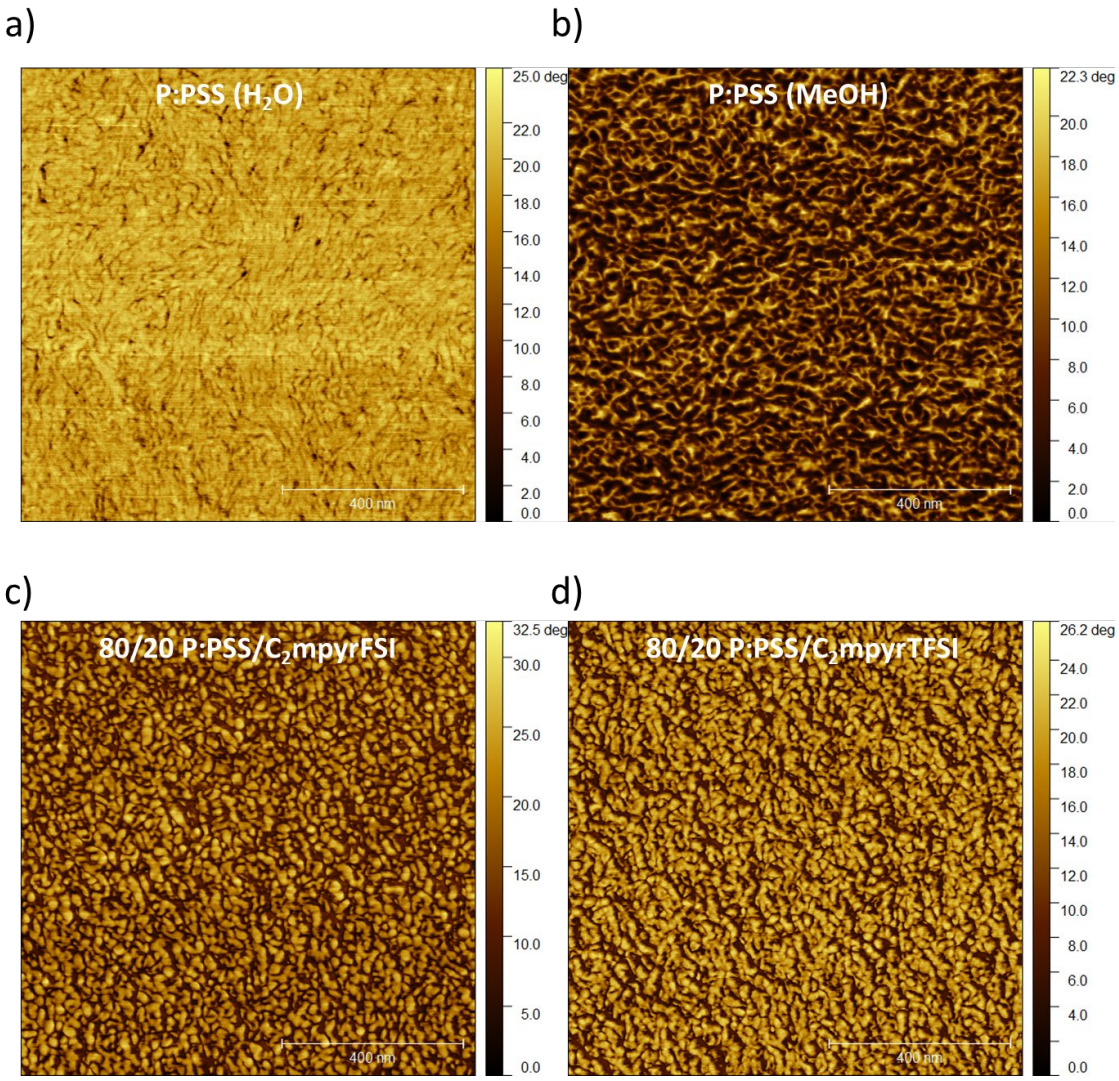

Figure S6. Phase AFM images of different a) PEDOT:PSS (H_2O), b) P:PSS (MeOH), c) 80/20 P:PSS/C_2mpyrFSI and d) 80/20 P:PSS/C_2mpyrTFSI composites.

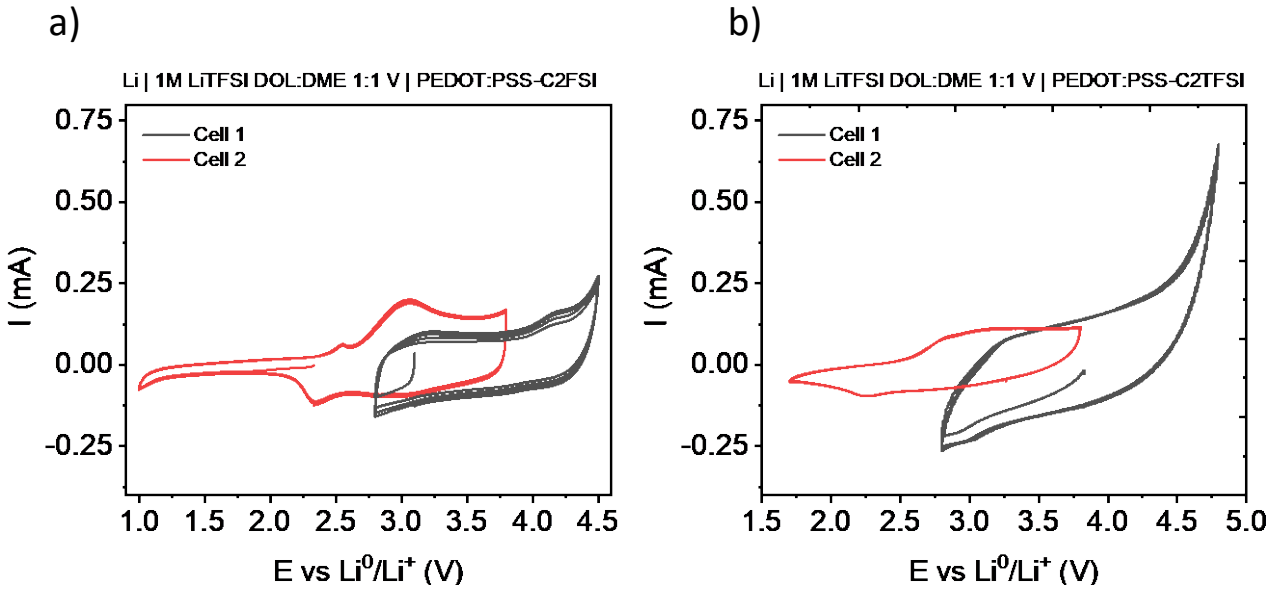

Figure S7. Electrochemical window in lithium metal cells of a) 80/20 P:PSS/C_2mpyrFSI and b) 70/30 P:PSS/C_2mpyrTFSI using 1M LiTFSI in DOL:DME 1:1 v at 10 mV s^{-1}.

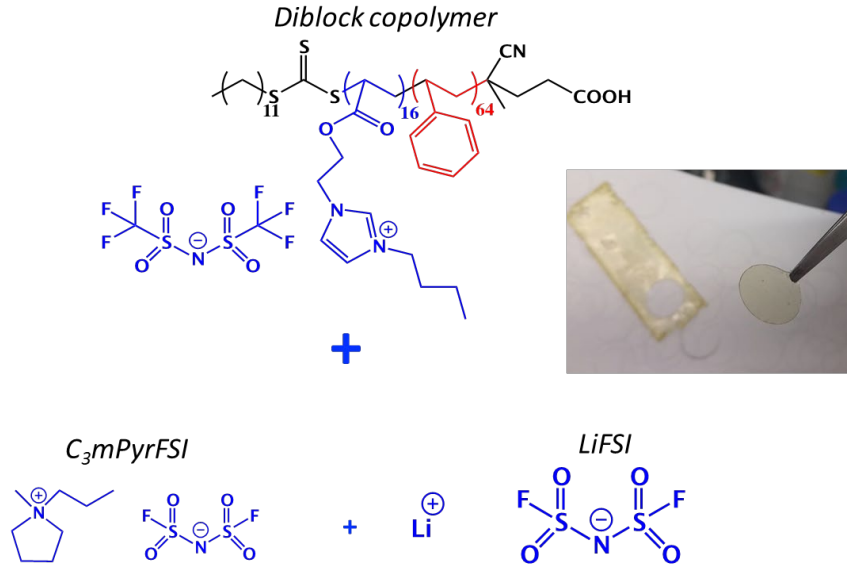

Figure S8. Chemical structures of solid electrolyte components: PILBLOC copolymer, C_3mpyrFSI and LiFSI.

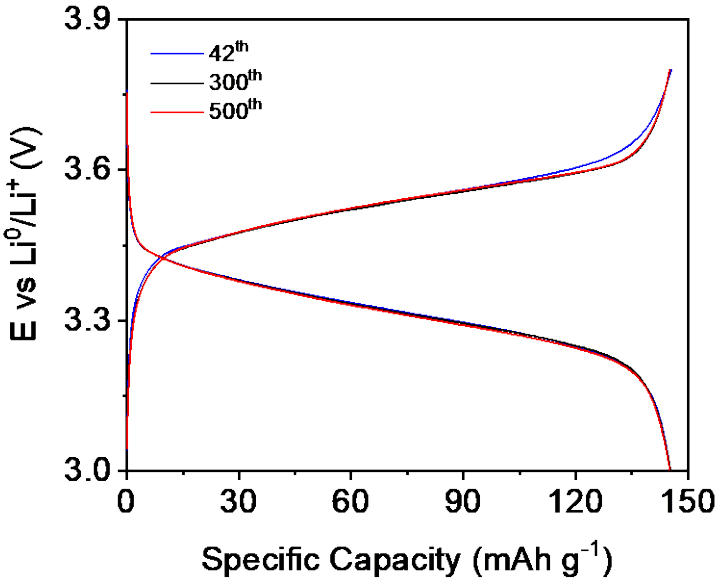

Figure S9. Voltage profile of OMIEC binder based cell of different cycles of the long term cycling from the beginning (42th).

Table S2. Literature review of solid state Li|LFP cells based on inorganic and polymer electrolytes.

Electrolyte	Cathode formulation [LFP/C_{65}/ionic binder] Ref.	Current density [mAh cm^{-2}] / LFP loading [mg cm^{-2}]	C rate	Specific capacity [mAh g^{-1}]	Cycling life
Diblock-EC-LiFSI[a]	60/10/30 [4]	0.046 / 2.7	C/10	150	100
PPE-PEO-PPE (LiTFSI)[b]	60/10/30 [5]	0.051 / 3	C/10	112	100
P(EO-co-PO)[c]	70/15/15 [6]	0.034 / 2	C/10	159	50
LAGP[d]	50/5/45 [7]	0.272 / 8	C/5	120	50
Diblock-IL-LiFSI[e]	60/40 P:PSS-OIPC-LiFSI This work	0.1 / 1.2	C/2	145	150
Diblock-IL-LiFSI[e]	60/10/30 PILBLOC-IL-LiFSI This work	0.1 / 1.2	C/2	130	55
PEO (LiTFSI)[f]	60/15/25 [8]	0.128 / 1.5	C/2	122	150
PI/DBDPE/PEO/LiTFSI[g]	60/15/25 [8]	0.128 / 1.5	C/2	143	300
LPO-LLZO[h]	50/5/45 [9]	0.1 / 1	1.5 C	120	400

[a]Poly(ionic liquid) – ethylene carbonate – LiFSI.
[b]Crosslinked poly(ethylene oxide-co-polyphosphoester) – LiTFSI
[c]Poly(ethylene oxide) – LiTFSI
[d]$Li_{1.5}Al_{0.5}Ge_{1.5}(PO_4)_3$
[e]Poly(ionic liquid) – C_3mpyrFSI – LiFSI
[f]Poly(ethylene oxide-co-polypropylene oxide) – LiTFSI
[g]Polyimide – decabromodiphenyl ethane – poly(ethylene oxide) – LiTFSI
[h]Li_3PO_4 – $Li_{6.5}La_3Zr_{1.5}Ta_{0.5}O_{12}$

References

1. M. B. Mcdonald and P. T. Hammond. Efficient Transport Networks in a Dual Electron/Lithium-Conducting Polymeric Composite for Electrochemical Applications. *ACS Appl. Mater. Interfaces* **2018**;10:15681–15690.
2. S. Wang, M. Yan, Y. Li, C. Vinado and J. Yang. Separating electronic and ionic conductivity in mix-conducting layered lithium transition-metal oxides. *J. Power Sources* **2018**;393:75–82.
3. R. Del Olmo, M. Forsyth and N. Casado. Mixed Ionic-Electronic Conductors Based on Polymer Composites BT - Advances in Nanocomposite Materials for Environmental and Energy Harvesting Applications. eds. A. E. Shalan, A. S. Hamdy Makhlouf and S. Lanceros-Méndez, Springer International Publishing, Cham, **2022**., pp. 493–532.
4. T. C. Mendes, N. Goujon, N. Malic, A. Postma, J. Chiefari, H. Zhu, P. C. Howlett and M. Forsyth. Polymerized Ionic Liquid Block Copolymer Electrolytes for All-Solid-State Lithium-Metal Batteries. *J. Electrochem. Soc.* **2020**;167:070525.
5. J. Olmedo, L. Meabe, R. Riva, G. Guzmán-González, L. Porcarelli, M. Forsyth, A. Mugica, I. Calafel, A. Muller, P. Lecomte, C. Jerome and D. Mecerreyes. Flame Retardant Polyphosphoester Copolymers as Solid Polymer Electrolyte for Lithium Batteries. *Polym. Chem.* **2021**.
6. S. T. Hsu, B. T. Tran, R. Subramani, H. T. T. Nguyen, A. Rajamani, M. Y. Lee, S. S. Hou, Y. L. Lee and H. Teng. Free-standing polymer electrolyte for all-solid-state lithium batteries operated at room temperature. *J. Power Sources* **2020**;449:227518.
7. A. Paolella, X. Liu, A. Daali, W. Xu, I. Hwang, S. Savoie, G. Girard, A. G. Nita, A. Perea, H. Demers, W. Zhu, A. Guerfi, A. Vijh, G. Bertoni, G. C. Gazzadi, G. Berti, C. Sun, Y. Ren, K. Zaghib, M. Armand, C. Kim, G. Xu and K. Amine. Enabling High-Performance NASICON-Based Solid-State Lithium Metal Batteries Towards Practical Conditions. *Adv. Funct. Mater.* **2021**;2102765:2102765.
8. Y. Cui, J. Wan, Y. Ye, K. Liu, L. Y. Chou and Y. Cui. A Fireproof, Lightweight, Polymer-Polymer Solid-State Electrolyte for Safe Lithium Batteries. *Nano Lett.* **2020**;20:1686–1692.
9. T. Deng, X. Ji, Y. Zhao, L. Cao, S. Li, S. Hwang, C. Luo, P. Wang, H. Jia, X. Fan, X. Lu, D. Su, X. Sun, C. Wang and J. G. Zhang. Tuning the Anode–Electrolyte Interface Chemistry for Garnet-Based Solid-State Li Metal Batteries. *Adv. Mater.* **2020**;32:1–10.